Journal of Cerebral Blood Flow & Metabolism (2009) 29, 1346–1357

www.jcbfm.com

Signal separation and parameter estimation in noninvasive dual-tracer PET scans using reference-region approaches

Aniket D Joshi[1,2], Robert A Koeppe[1], Jeffrey A Fessler[1,2,3] and Michael R Kilbourn[1]

[1]*Division of Nuclear Medicine, Department of Radiology, University of Michigan, Ann Arbor, Michigan, USA;* [2]*Department of Biomedical Engineering, College of Engineering, University of Michigan, Ann Arbor, Michigan, USA;* [3]*Department of Electrical Engineering and Computer Science, College of Engineering, University of Michigan, Ann Arbor, Michigan, USA*

This is the first study to report results from a noninvasive dual-tracer positron emission tomography (PET) in humans not requiring arterial sampling, in which two radiotracers were injected closely in time within the same scan. These studies yield near simultaneous information on two different neuropharmacological systems, providing better characterization of a subject's neurologic condition. The noninvasive dual-tracer approach described in this study is based on the primary assumption that an appropriate bolus plus constant infusion protocol brings the reference tissue of the first radiotracer to steady state before injection of the second tracer. Two methods for separation of time–activity curves (TACs) and parameter estimation were investigated, namely (1) an extrapolation method, in which TACs of the first tracer were extrapolated over total scan duration followed by subtraction from dual-tracer TACs and (2) a simultaneous fitting method, in which reference-region models for both tracers were fitted simultaneously to dual-tracer TACs. Combinations of two reversible tracers ([^{11}C]flumazenil and [^{11}C]dihydrotetrabenazine) or one reversible and one irreversible tracer ([^{11}C]*N*-methylpiperidinyl propionate) were used. After the dual-tracer scan, a single-tracer (ST) scan using one of the tracers was obtained for comparison of the dual-tracer results. Both approaches provided parameter estimates with intersubject regions-of-interest means typically within 10% of those obtained from ST scans without an appreciable increase in variance.
Journal of Cerebral Blood Flow & Metabolism (2009) **29,** 1346–1357; doi:10.1038/jcbfm.2009.53; published online 29 April 2009

Keywords: PET; tracer kinetics; *in vivo* neuropharmacology; dual-tracer; carbon-11

Introduction

Dual-tracer positron emission tomography (PET) methodology provides an opportunity to characterize two different neuropharmacological aspects of a subject from a single PET acquisition. Typically, measurement of two different pharmacological aspects using PET would involve two separate single-tracer (ST) PET scans. The dual-tracer methodology can obtain data related to two systems of interest almost simultaneously by injecting two tracers separated closely in time within a single PET scan. Dual-tracer PET data analysis presents a challenge as all positron-emitting isotopes emit photons with 511 keV of energy, and it is not possible to separate the signals from the two tracers using differing energy windows. Injecting two tracers simultaneously would make it impossible to separate the two signals; hence, tracer injections in this work were staggered in time by 20 or 30 mins.

The earliest work in dual-tracer PET was carried out in phantom studies, in which differences in tracer half-lives were used for signal separation (Huang *et al*, 1982). Koeppe *et al* (2001) reported the first results of dual-tracer brain PET studies in humans using ^{11}C-labeled tracers, in which tracer models were fitted simultaneously to estimate the parameters of both tracers using metabolite-corrected arterial plasma input functions. Kadrmas and Rust (2005) evaluated the possibility of a similar parallel-model fitting approach in a simulation study for rapid dual-tracer scans. Various applications of rapid dual-tracer studies have been described recently,

Correspondence: Dr RA Koeppe, University of Michigan, Department of Radiology, Division of Nuclear Medicine, 3480 Kresge III 0552, Ann Arbor, MI, 48109-0552, USA.
E-mail: koeppe@umich.edu
Received 7 January 2009; revised 7 April 2009; accepted 8 April 2009; published online 29 April 2009

including simulation studies for measuring hypoxia and blood flow (Rust *et al*, 2006) and tumor characterization using ^{62}Cu-PTSM (pyruvaldehyde-bis[*N*4-methylthiosemicarbazone]) and ^{62}Cu-ATSM (diacetyl-bis[*N*4-methylthiosemicarbazone]) in dogs (Black *et al*, 2008).

The existing work on dual-tracer studies mentioned above is based on an arterial sampling approach, which is inconvenient for the subjects because of its invasive nature and is difficult owing to the requirement of plasma metabolite correction for each of the two tracers. This paper reports results of a new noninvasive, dual-tracer brain PET approach in humans on the basis of a reference tissue model instead of an arterial plasma input function model.

The possibility of analysis of dual-tracer studies without arterial sampling was first explored in Koeppe *et al* (2004). In this paper, we have extended this original work and have reported two reference tissue methods for separating the individual-tracer signals and estimating parameters of interest, such as (1) an extrapolation method (EM), in which time–activity curves (TACs) of the first tracer were extrapolated over total scan duration followed by subtraction from dual-tracer TACs and (2) a simultaneous fitting method (SM), in which reference-region models for both tracers were fitted simultaneously to dual-tracer TACs. The pharmacological indices of interest in the dual-tracer studies were the blood–brain barrier transport parameter (R_1), distribution volume ratio for reversible tracers ($DVR = BP_{ND} + 1$ where BP_{ND} is the nondisplaceable binding potential (Innis *et al*, 2007)), and k_3 (the trapping constant), for irreversible tracers.

In this work, we have attempted to minimize the variance in the parametric images by implementing the following three steps: (1) noise reduction in TACs by an adaptive smoothing approach; (2) reduction in the number of parameters to be fitted by fixing the k_4 parameter for both tracers to their population average in the full-reference tissue model for reversible tracers (Cunningham *et al*, 1991; Lammertsma *et al*, 1996); and (3) application of robust linear estimation techniques, such as the Logan analysis to ST curves extracted from dual-tracer data. Each of these steps is described in detail in the Materials and methods section.

The dual-tracer scans were also followed by the ST scan of one of the tracers to provide a 'gold standard' for comparison of dual-tracer results. The parametric images obtained from dual-tracer studies were in good agreement with ST studies with similar noise properties and intersubject regions-of-interest means typically within 10%.

Materials and methods

Radiotracers

The radiotracers used in this study have been well characterized for traditional ST PET scans at our institution; these included flumazenil ([^{11}C]FMZ), a benzodiazepine receptor antagonist (Holthoff *et al*, 1991; Koeppe *et al*, 1991); dihydrotetrabenazine ([^{11}C]DTBZ), a ligand for the vesicular monoamine transporter 2 (VMAT2) binding site (Koeppe *et al*, 1999*a*; Koeppe *et al*, 1997; Koeppe *et al*, 1996); and *N*-methylpiperidinyl propionate ([^{11}C]PMP), a substrate for hydrolysis by the enzyme, acetylcholinesterase (AChE) (Koeppe *et al*, 1999*b*). Both [^{11}C]FMZ and [^{11}C]DTBZ can be classified as reversible tracers and have been analyzed successfully using both bolus and bolus plus continuous infusion protocols (Frey *et al*, 1993; Koeppe *et al*, 1997). [^{11}C]PMP can be classified as an irreversible tracer.

Key Assumption

The key assumption in noninvasive dual-tracer PET is that an appropriate bolus plus constant infusion protocol for the first tracer brings its reference region to steady state before the injection of the second tracer. Simply put, the fate of the reference region of the first tracer is assumed to be known as its concentration is constant from the time the second tracer is injected until the end of the scan despite 'contamination' by the second tracer (Koeppe *et al*, 2004). The more rapidly reversible a tracer is, the more likely for this key assumption to hold true.

Data Acquisition, Reconstruction, and Processing

Dual-tracer studies were carried out in 37 healthy individuals using the following two tracer pairs: (1) [^{11}C]FMZ and [^{11}C]DTBZ, or (2) [^{11}C]FMZ and [^{11}C]PMP. Table 1 summarizes the details, such as the order in which the tracers were injected, the time difference between tracer injections, and the ST scan that followed the dual-tracer scan. The irreversible tracer, [^{11}C]PMP, has no region of negligible trapping; thus, only [^{11}C]FMZ and [^{11}C]DTBZ, with the pons and occipital cortex as reference regions, respectively, were used as first tracers in this work, whereas [^{11}C]PMP was used exclusively as a second tracer. For studies in which [^{11}C]FMZ was injected first, studies were carried out with two delay windows between tracer injections (20 and 30 mins). It was not possible to reliably achieve steady state in the occipital cortex, the reference tissue for [^{11}C]DTBZ, by 20 mins. Hence, studies in which [^{11}C]DTBZ was injected first were carried out with a 30-min injection offset. The injected radioactivities were approximately the same for both tracers. In all, 12 mCi (444 MBq) ± 10% of each tracer was administered. Scan data were acquired for 80 mins as a dynamic sequence of 26 or 27 frames for 20- or 30-min offsets, respectively. The dual-tracer studies were followed by a 60-min ST scan using one of the tracers used in the dual-tracer study. Each ST scan provided a 'gold standard' for comparison with one of the tracers from the dual-tracer scan. Single-tracer studies were not carried out for both the dual-scan tracers because of time and dosimetry constraints.

Table 1 Imaging protocol details for dual-tracer studies

Dual-tracer scans[a]	*Time difference between tracer injections*	*Single-tracer scan following the dual-tracer scan*	*Number of subjects*
[^{11}C]FMZ/[^{11}C]DTBZ	20	FMZ	2
		DTBZ	2
		FMZ	1
		DTBZ	1
	30	FMZ	1
		DTBZ	2
		FMZ	2
		DTBZ	1
[^{11}C]DTBZ/[^{11}C]FMZ	30	FMZ	2
		DTBZ	2
		FMZ	1
		DTBZ	1
[^{11}C]FMZ/[^{11}C]PMP	20	FMZ	5
		PMP	5
	30	FMZ	4
		PMP	5

[^{11}C]DTBZ, dihydrotetrabenazine; [^{11}C]FMZ, flumazenil; [^{11}C]PMP, *N*-methylpiperidinyl propionate.
[a]Injection order.

The ST scans were also used to assess the validity of the key assumption that the reference tissue of the first tracer reached steady state before the second tracer was administered.

All PET scans were acquired in a three-dimensional mode on an ECAT EXACT HR + tomograph (Siemens Medical Systems, Inc., Knoxville, TN, USA). Images were reconstructed using Fourier rebinning (Defrise *et al*, 1997) of the three-dimensional data into two-dimensional sinograms and ordered subsets expectation maximization (Comtat *et al*, 1998; Hudson and Larkin, 1994) using 4 iterations and 16 subsets.

Subject motion across frames was corrected using Neurostat (University of Washington, Seattle, Washington), initially developed at the University of Michigan (Minoshima *et al*, 1994; Minoshima *et al*, 1993). Scans were reoriented to the stereotactic atlas of Talairach and Tournoux (1988), followed by both linear scaling and nonlinear warping.

All modeling estimations were performed voxel-by-voxel, creating parametric images of the blood–brain barrier transport parameter (R_1), the *DVR* (= 1 + BP_{ND}; Innis *et al*, 2007) for the reversible tracers, and a 'trapping rate' parameter (k_3) for the irreversible tracer. Volumes of interest were obtained using a standardized volume-of-interest template defined in the Talairach atlas space.

Dual-Tracer Signal Separation Techniques

The proposed reference tissue-based dual-tracer approach is suitable for cases, in which the injected first tracer has a tissue or a region with negligible receptor binding or trapping. We first describe the methods for the case, in which both injected radiotracers bind reversibly and then extend it to the case, in which the first tracer has reversible binding and the second tracer has irreversible trapping.

In the case of a reversible ST two-tissue compartment model, the target region concentration time courses or TACs can be expressed in terms of the model rate constants and reference-region concentration time course using the full-reference tissue input model equation shown in Equation (1) as (Cunningham *et al*, 1991; Lammertsma *et al*, 1996)

$$y_i(t) = R_1(y_r(t) + ay_r(t) \otimes e^{-ct} + by_r(t) \otimes e^{-dt}) \quad (1)$$

where y_i (t) is the target region concentration time course for region or voxel i, y_r (t) the reference-region concentration time course, and R, a, b, c, and d model parameters that are functions of the rate constants of a two-tissue compartment model, K_1–k_4 and K_1^{ref} (K_1–k_4 are the rate constants of a two-tissue compartment model and K_1^{ref} is the transport parameter for the reference region). The PET TACs are obtained by binning the instantaneous PET data over N temporal frames. The target region, TAC, binned into N temporal frames can be enumerated for voxel i as $\bar{y}_i = [y_i^1 \ldots y_i^N]$, where $y_i^j = (1/t_{end}^j - t_{start}^j) \int_{t_{start}^j}^{t_{end}^j} y_i(t)\,dt$ and t_{start}^j and t_{end}^j are the start and end times of the jth frame. The reference-region TAC vector, $\bar{y}_r$, can also be obtained similarly. Model parameters can be arranged in a parameter vector form as follows:

$$\bar{\theta}_i = [\frac{K_1}{K_1^{ref}},\ k_2,\ k_3,\ BP_{ND}]_i \quad (2)$$

where $BP_{ND} = k_3/k_3$. Using Equations (1) and (2), we can express TAC ($\bar{y}_i$) as a function of the reference-region TAC ($\bar{y}_r$) and the parameter vector ($\bar{\theta}_i$) plus a residual error term ($\bar{\varepsilon}_i$) as shown below.

$$\bar{y}_i = f(\bar{y}_r, \bar{\theta}_i) + \bar{\varepsilon}_i \quad (3)$$

The parameter vector can be estimated using nonlinear least-squares to minimize the difference

between the model-predicted and measured data:

$$\hat{\bar{\theta}}_i = \arg\min_{\theta_i} \left\| \bar{y}_i - Wf(\bar{y}_r, \bar{\theta}_i) \right\|_2^2 \quad (4)$$

where W is the weighting matrix that takes into account the difference in variance between different frames of the PET scan. The normalized variance for the jth frame is given by $\sigma_j^2 = y_i^j e^{\lambda T_j} / t_{\text{end}}^j - t_{\text{start}}^j$ (Logan *et al*, 2001) where T_j is the midpoint time for the jth frame and λ the known tracer decay constant ($\lambda = 0.0347$/min for ^{11}C tracers). The weighting matrix, $W \in R^{N \times N}$, is a diagonal matrix with $1/\sigma_j^2$ along the diagonal (Faraway, 2004).

The above Equations (1) to (4) are derived for a ST. In a dual-tracer study, two tracers are injected; Tracer II was injected at time $t = T'$ after Tracer I. The dual-tracer TAC ($\bar{y}_i$) can be represented as

$$\bar{y}_i = \bar{y}_i^{\text{I}} + \bar{y}_i^{\text{II}} + \bar{\varepsilon}_i \quad (5)$$

where $\bar{y}_i^{\text{I}}$ and $\bar{y}_i^{\text{II}}$ are the constituent individual-tracer signals and $\bar{\varepsilon}_i$ the noise vector.

This work investigated two methods for estimating the individual-tracer curves ($\bar{y}_i^{\text{I}}$ and $\bar{y}_i^{\text{II}}$) and their parameter vectors ($\bar{\theta}_i^{\text{I}}$ and $\bar{\theta}_i^{\text{I}}$) from the dual-tracer signal $\bar{y}_i$, namely EM and SM.

Extrapolation Method: The EM is based on the original approach reported in Koeppe *et al* (2004), in which the simplified reference tissue model (Lammertsma and Hume, 1996) was used to extrapolate the first tracer, whereas in this case, we use the full-reference tissue model. Data exclusive to Tracer I are known for $t < T'$, the injection time of Tracer II. Using this early data, Tracer I parameter vector for each voxel i ($\bar{\theta}_i^{\text{I}}$) could be estimated by minimizing the cost function shown below using some nonlinear estimation algorithm.

$$\hat{\bar{\theta}}_i^{\text{I}} = \arg\min_{\bar{\theta}_i^{\text{I}}} \left\| \bar{y}_i^{\text{I}} - Wf(\bar{y}_r^{\text{I}}, \bar{\theta}_i^{\text{I}}) \right\|_2^2 \quad (6)$$

However, this minimization required nonlinear estimation of the four parameters from just 20 mins of data which gave noisy estimates. To counter this problem, the parameter of interests, R_1 (K_1/K_1^{ref}) and DVR ($= 1 + BP_{\text{ND}}$) for Tracer I, were first estimated by using the principal component analysis (PCA)-based reference-region Logan plot analysis (Joshi *et al*, 2008) from the first 20 mins. The remaining unknown elements of the parameter vector, $\bar{\theta}_i^{\text{I}}$ (k_2, k_4), were estimated using nonlinear least squares from Equation (6). Using this parameter vector and the reference-region TAC for Tracer I, Tracer I TACs were extrapolated until the end of the scan duration using the full-reference tissue model ($\hat{\bar{y}}_i^{\text{I}} = f(\bar{y}_r^{\text{I}}, \hat{\bar{\theta}}_i^{\text{I}})$). Tracer II component was isolated by subtracting the extrapolated Tracer I signal from the dual-tracer TAC for all voxels i ($\hat{\bar{y}}_i^{\text{II}} = \bar{y}_i - \hat{\bar{y}}_i^{\text{I}}$). The isolated Tracer II curves ($\hat{\bar{y}}_i^{\text{II}}$) also included the reference-region curve for Tracer II ($\hat{\bar{y}}_r^{\text{II}}$) and hence, all the information to estimate the parameter of interest for Tracer II (DVR and R_1) using the PCA-based Logan analysis has been obtained.

Simultaneous Fitting Method: A potential drawback of the two-step EM described above is that errors in the parameter estimation of Tracer I from limited early data propagate into parameter estimates of Tracer II. There may be cases, in which error in Tracer I estimates could propagate in such a way to give physiologically improbable parameter values for Tracer II. Thus, as an alternative to the two-step EM, we also explored a one-step approach, in which the parameters of both the tracers were estimated at the same time by fitting the dual-tracer TACs to the reference tissue models of both tracers simultaneously.

This SM attempted to estimate the model parameters for both tracers using one minimization operation. We first applied the EM to the dual-tracer curve of Tracer II reference region alone, to isolate the Tracer II reference-region curve ($\hat{\bar{y}}_r^{\text{II}}$). The Tracer I reference-region TAC ($\bar{y}_r^{\text{I}}$) was known by virtue of the primary assumption. Using the reference-region curves for both tracers, the voxelwise parameter vectors for both the tracers could be estimated simultaneously by minimizing the following cost function:

$$(\hat{\bar{\theta}}_i^{\text{I}}, \hat{\bar{\theta}}_i^{\text{II}}) = \arg\min_{(\theta_i^{\text{I}}, \theta_i^{\text{II}})} \times \left\| \bar{y}_i - W\{f(\bar{y}_r^{\text{I}}, \bar{\theta}_i^{\text{I}}) + f(\hat{\bar{y}}_r^{\text{II}}, \bar{\theta}_i^{\text{II}})\} \right\|_2^2 \quad (7)$$

The primary parameter of interest (DVR) for both tracers could now be calculated directly from the estimated parameter vectors, $\hat{\bar{\theta}}_i^{\text{I}}$ and $\hat{\bar{\theta}}_i^{\text{II}}$.

Using an Irreversible Tracer as Tracer II

The methods described above were for the case, in which both the injected tracers bind reversibly, although they can easily be extended to the case, in which Tracer II has irreversible kinetics. However, in the case of an irreversible tracer, the reference region-based model equations for the TACs will be different from those for a reversible tracer (Equation (1)).

The differential equations for an irreversible two-tissue compartment model are given as ($k_4^{\text{II}} = 0$ in Figure 1)

$$\frac{dC_{ND}(t)}{dt} = K_1 C_p(t) - (k_2 + k_3) C_{ND}(t), \quad (8)$$

$$\frac{dC_S(t)}{dt} = k_3 C_{ND}(t) \quad (9)$$

where $C_p(t)$ is the arterial plasma input, $C_{ND}(t)$ the radioligand concentration in the nondisplaceable compartment, $C_S(t)$ the radioligand concentration in the specific compartment, and K_1, k_2, and k_3 the kinetic parameters of the model with k_3, the trapping constant, being the parameter of interest to be estimated from the dynamic data. In the case of the arterial sampling approach, the solution for total tracer concentration in tissue ($y_i = C_{ND} + C_S$) is given

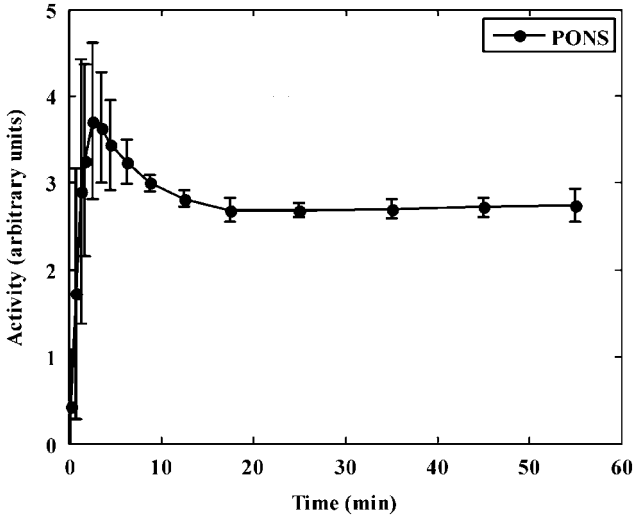

Figure 1 Average time–activity curve (TAC) for the pons, the reference tissue for [^{11}C]FMZ, from seven subjects who underwent a 60-min single-tracer [^{11}C]FMZ scan. TACs have been scaled such that the area under the curve is the same for all subjects to account for differences in absolute radioactivity levels. Error bars represent the s.d. of the TACs for the seven subjects and indicate the degree of variability in maintaining steady-state conditions.

below (Herholz *et al*, 2001)

$$y_i(t) = \frac{K_1 k_2}{k_2 + k_3} \int_0^t C_p(\tau)\, \mathrm{e}^{-(k_2+k_3)(t-\tau)}\, \mathrm{d}\tau + \frac{K_1 k_3}{k_2 + k_3} \times \int_0^t C_p(\tau)\, \mathrm{d}\tau \quad (10)$$

where $C_p(\tau)$ denotes the arterial input function. For the case of an irreversible tracer like [^{11}C]PMP, the basis for the reference tissue approach is not that the reference tissue is void of specific uptake, but in fact the opposite, that the reference tissue has such a high rate of irreversible trapping that all the tracer that enters the reference tissue is trapped and none clears back into the blood. Thus, we assume that the TAC of the reference tissue, which is the basal ganglia for [^{11}C]PMP, is proportional to the integral of the arterial input function. Kinetic studies of [^{11}C]PMP indicate that only $\sim$10% of the tracer entering the basal ganglia clears back to tissue, whereas $\sim$90% is irreversibly trapped (Koeppe *et al*, 1999*b*).

The irreversible tracer, TAC, from a region with an extremely high k_3 value (e.g., the striatum for [^{11}C]PMP) is assumed to equal the time integral of the arterial input function multiplied by the transport rate constant of the reference region, K_1^{ref} (Herholz *et al*, 2001; Nagatsuka *et al*, 2001)

$$y_r(t) = K_1^{ref} \int_0^t C_p(\tau)\mathrm{d}\tau \quad (11)$$

Equation (11) was rearranged to get an expression for the plasma input function in terms of the reference-region curve as shown below:

$$C_p(t) = \frac{1}{K_1^{ref}} \frac{\mathrm{d}y_r(t)}{\mathrm{d}t} \quad (12)$$

The differentiation operation in Equation (12) was performed by interpolating the reference-region curve on a fine grid followed by numerical differentiation. Substituting the expression for C_p (t) obtained from Equation (12) in Equation (10) yielded

$$y_i(t) = \left(\frac{K_1}{K_1^{ref}}\right) \frac{k_2}{k_2 + k_3} \int_0^t \frac{\mathrm{d}y_r(\tau)}{\mathrm{d}\tau}\, \mathrm{e}^{-(k_2+k_3)(t-\tau)}\, \mathrm{d}\tau + \left(\frac{K_1}{K_1^{ref}}\right) \frac{k_3}{k_2 + k_3} y_r(t) \quad (13)$$

which expresses the target tissue curve in terms of the reference tissue curve and the rate parameters for irreversible tracers and is equivalent to Equation (1) for reversible tracers.

Using the notation derived for reversible tracers, the TAC for an irreversible tracer can be expressed as $\bar{y}_i = f(\bar{y}_r, \bar{\theta}_i) + \bar{\varepsilon}_i$, where $\bar{y}_i$ is the tissue TAC, $\bar{y}_r$ the reference-region curve, $\bar{\theta}_i = [K_1/K_1^{ref}, k_2, k_3]$ the parameter vector for irreversible tracers, and the function f the reference tissue model in Equation (13).

After signal separation, the parameter of interest for the irreversible tracer (k_3) was estimated by the reference region-based linear least squares method (RLS) as proposed in Nagatsuka *et al* (2001). The operational equation of RLS is shown below.

$$\bar{y}_i(T) = \rho_1 \bar{y}_r(T) + \rho_2 \int_0^T \bar{y}_r(\tau)\mathrm{d}\tau + \rho_3 \int_0^T \bar{y}_i(\tau)\mathrm{d}\tau \quad (14)$$

where ρ_1, ρ_2, and ρ_3 are the coefficients of the linear model above and $k_3 = \rho_2/\rho_1$.

Robust Parameter Estimation

To improve the robustness of the parameters of interest obtained from the noninvasive dual-tracer PET, the following three procedures were developed and implemented:

Adaptive Smoothing: In this step, a spatially dependent smoothing protocol was implemented to reduce noise in TACs before the signal separation and parameter estimation steps. The neighborhood of the voxel's TAC under consideration (y_i) was searched to identify those TACs that had shapes similar to those of y_i. An average of the TAC under consideration and the qualifying neighboring TACs yielded a TAC with reduced noise. This approach caused little smoothing in regions with kinetically distinct voxels, thus preserving spatial resolution. The procedure is mathematically represented below:

A set of voxel indices, N_i, was selected for the voxel i under consideration, such that

$$N_i = \{j : \|y_i - y_j\|_2 < T\} \quad (15)$$

where y_j is the TAC of a neighboring voxel j, $||y_i - y_j||_2$ the L_2-norm of the difference vector between y_i and y_j, and T the threshold for the L_2-norm and was chosen to be 10% of $||y_i||_2$. This threshold was chosen as it gave the best trade-off between noise reduction and preservation of spatial resolution. This search was performed in a $3 \times 3 \times 3$ neighborhood of voxel i. Once such a set of TACs was chosen, an average TAC was calculated (y_i^{AVG}), which had less noise than the original dual-tracer TAC (y_i) and was used for curve separation and parameter estimation. This step was applied to both dual-tracer and ST scans.

Population Average k_4 in the Full-Reference Tissue Model: Another step used to improve precision in the separation of the individual-tracer components and hence, in the binding parameters, was reducing the complexity of the full-reference tissue model by fixing the k_4 parameter for each tracer to its respective population average value. Our overall goal was to estimate DVR ($= 1 + BP_{ND}$) for each tracer. As $BP_{ND} = k_3/k_4$ ratio, it may seem that using the simplified reference tissue model, in which only $1 + BP_{ND}$ is estimated instead of k_3 and k_4 separately, would accomplish the same goal. However, the simplifying assumption in the simplified reference tissue model is instantaneous equilibration between free and specific compartments, which implies very high values for both k_3 and k_4. This assumption may bias the shapes of the individual tissue curves for the tracers used in this work. By fixing the k_4 values to the population average values, we reduce the complexity of the full-reference tissue model, as in simplified reference tissue model, but constrain the individual-tracer TACs to more closely approximate their true shapes.

Signal Separation Followed by Estimation of Binding Measures: For SM, the binding index could be calculated directly from the individual model parameters of the k_4-constrained reference tissue model. However, direct calculation from the individual rate constants may still lack precision despite the adaptive smoothing and k_4 constraint. Instead, the reference tissue model fits to the dual-tracer data (Equation 12) were used only to extract the voxelwise TAC components for each of the two radiotracers. These separated TACs were then used with robust linear estimation methods to obtain final parametric images (the Logan graphical analysis for DVR estimation in reversible tracers and RLS for k_3 estimation in irreversible tracers).

As the process of signal separation for SM provides smooth TACs, the PCA-based Logan analysis is not required and the traditional Logan analysis is sufficient. Another point to be noted is that as the parameters of interest are estimated after signal separation, the accuracy of the shape of the TAC is of interest, and not the accuracy of the fitted parameter vectors, $(\hat{\theta}_i^{I}, \hat{\theta}_i^{II})$, in Equation 7. The minimization step in Equation 7 is an ill-posed problem with multiple solutions, but the shapes of the TACs obtained from each of these solutions of $(\hat{\theta}_i^{I}, \hat{\theta}_i^{II})$ are nearly identical.

Analysis of Single-Tracer Studies

For the analysis of ST studies, adaptive smoothing as described earlier was applied before parametric estimation. For reversible tracers, the parameters of interest (R_1 and DVR) were estimated using the PCA-based Logan plot analysis, and for the irreversible tracer, the parameters of interest (R_1 and k_3) were estimated using RLS.

Comparison of Dual-Tracer and Single-Tracer Results

Parametric estimates of DVR (for FMZ and DTBZ) and k_3 (for PMP) from the two dual-tracer approaches were compared with each other and also with ST estimates using paired Student's t-tests. The metric tested was the percentage differences between the estimates from different methods for all regions.

Results

Figure 1 shows the average TAC for the pons, (reference region for [^{11}C]FMZ) from seven ST [^{11}C]FMZ scans. The pons TAC for each subject has been normalized such that the area under the curve is the same for all subjects. These scans show that it is possible to maintain a steady state in the pons from the time the second tracer has been administered. The infusion protocol (35% bolus−65% infusion) was designed such that steady state was achieved by 20 mins, while obtaining reasonable counts in early frames. The error bars indicate s.d. of the tissue curve values across subjects. A slightly larger s.d. was seen toward the end of the scan, indicating that the reference tissue TAC of some subject may have deviated slightly from steady state. However, computer simulations have shown that the small deviations from steady state as those seen in Figure 1 are not expected to cause appreciable errors in the estimated parameters (results not shown).

Figure 2 shows the dynamic image sequence from a [^{11}C]FMZ–[^{11}C]DTBZ study, in which [^{11}C]DTBZ was injected as a bolus 20 mins after [^{11}C]FMZ. Figure 3 shows the parametric images estimated using EM from a [^{11}C]FMZ–[^{11}C]DTBZ dual-tracer study obtained with the same protocol as shown in Figure 2. The parametric images for both [^{11}C]FMZ

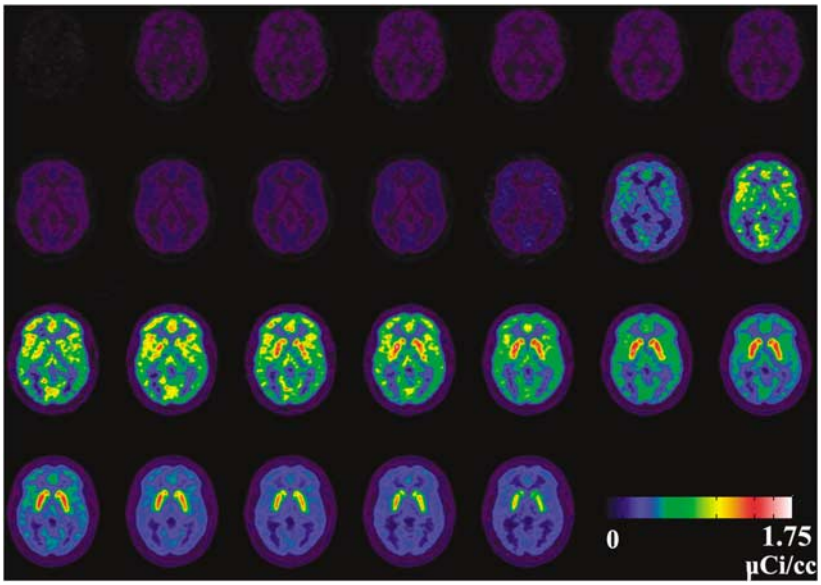

Figure 2 Dynamic dual-tracer PET image sequence for [^{11}C]FMZ–[^{11}C]DTBZ study with a 20-min offset. The frame sequence for the 80-min scan was 4×0.5 mins, 3×1.0 min, 2×2.5 mins, 2×5.0 mins, (second tracer injected at 20 mins), 4×0.5 mins, 3×1.0 min, 2×2.5 mins, 2×5 mins, and 4×10 mins frames. The second tracer is injected just before the 12th frame. It is noted that the much large apparent signal of [^{11}C]DTBZ is in part because of showing decay corrected data. Hence, the injection of the same dose of [^{11}C]DTBZ at 20 mins seemed twice as high relative to the [^{11}C]FMZ in the early frames.

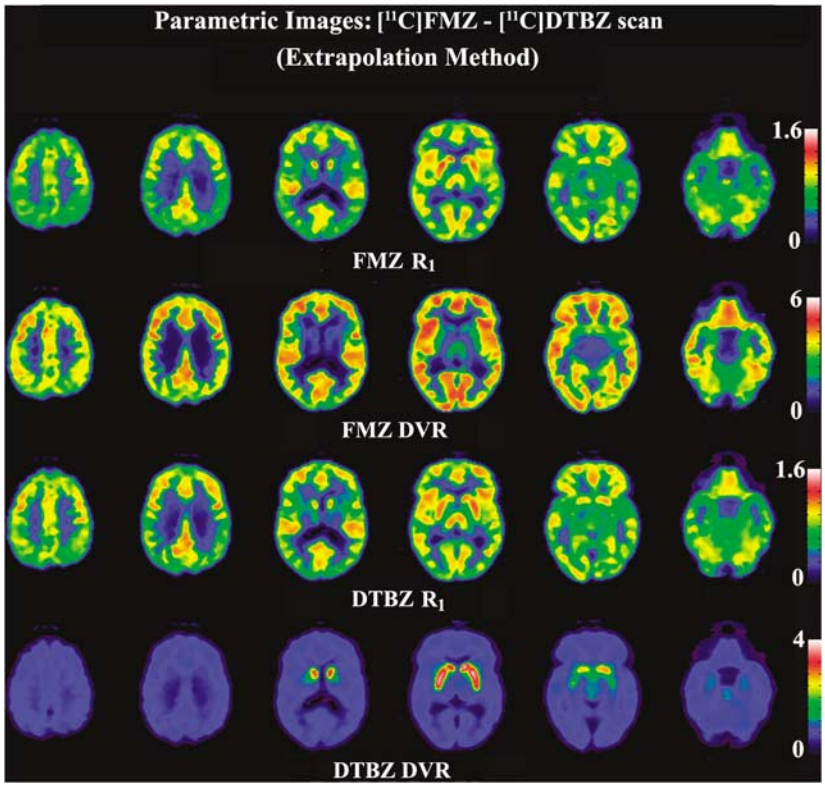

Figure 3 Parametric images obtained from a flumazenil ([^{11}C]FMZ)–dihydrotetrabenazine ([^{11}C]DTBZ) study at six brain levels. The parametric images shown are $R_1 = K_1/K_1^{ref}$ ratio (rows 1 and 3), and the distribution volume ratio ($DVR = 1 + BP_{ND}$) (rows 2 and 4) for both tracers.

(top two rows) and [^{11}C]DTBZ (bottom two rows) are shown for the relative blood–brain barrier transport rate, R_1 ($= K_1/K_1^{ref}$; rows 1 and 3) and the DVR ($= 1 + BP_{ND}$; rows 2 and 4).

[^{11}C]FMZ–[^{11}C]DTBZ Studies

Figure 4 (panel A) shows DVR images of three brain slices for studies with the same 20 mins FMZ:DTBZ

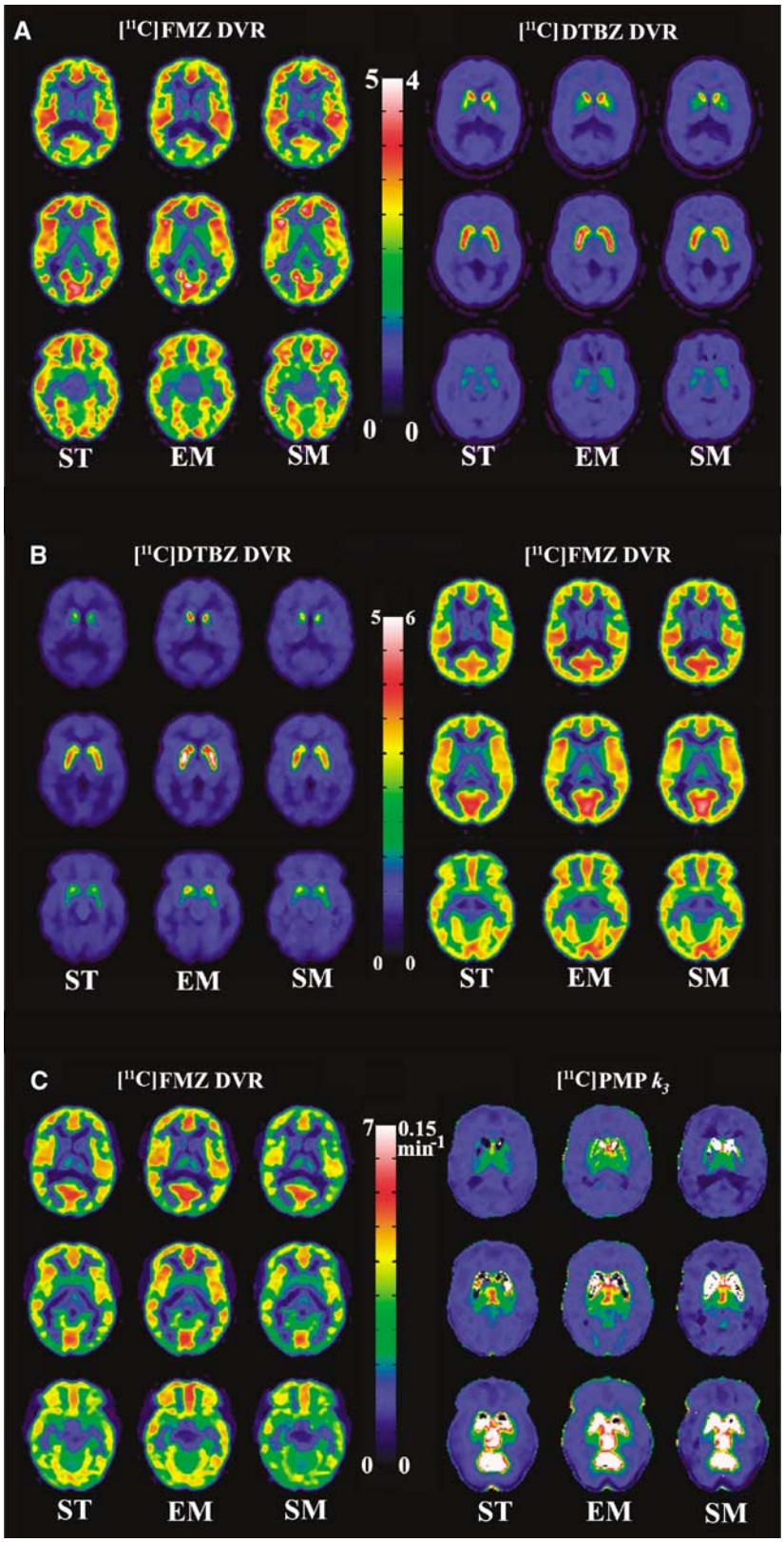

Figure 4 Comparison of parametric images of three brain levels from dual-tracer with those from single-tracer (ST) studies. The left-most column for each tracer is from a STstudy, which acts as a 'gold standard' for comparison of dual-tracer results. (**A**) flumazenil ([^{11}C]FMZ) injected 20 mins before dihydrotetrabenazine ([^{11}C]DTBZ). (**B**) [^{11}C]DTBZ injected 30 mins before [^{11}C]FMZ. (**C**) [^{11}C]FMZ injected 30 mins before [^{11}C]PMP. The extrapolation method (EM) and simultaneous fitting method (SM) show image patterns and magnitudes very close to those from the ST studies.

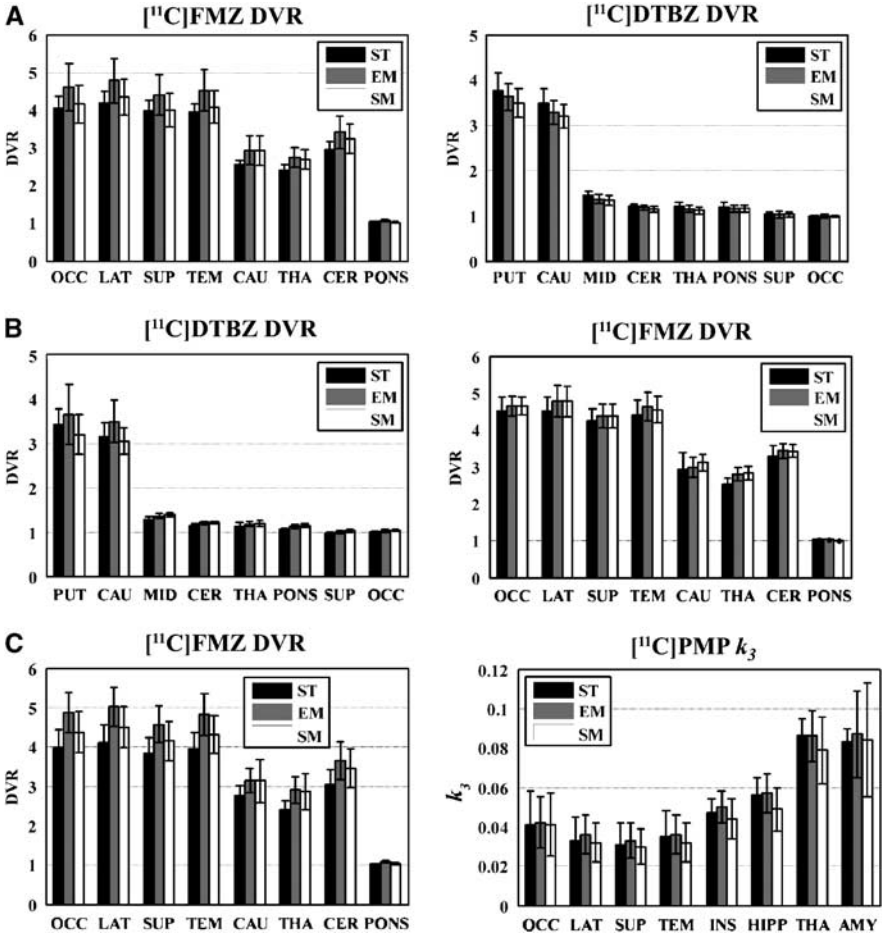

Figure 5 Comparison of intersubject means and s.d. in parametric estimates obtained from single-tracer (ST) and dual-tracer studies analyzed using extrapolation method (EM) and simultaneous fitting method (SM). Results from eight regions of interest extracted from parametric images are shown. (**A**) Comparison of dual-tracer flumazenil ([^{11}C]FMZ)–dihydrotetrabenazine ([^{11}C]DTBZ) studies ($n = 12$) with ST studies ($n = 6$). (**B**) Comparison of dual-tracer [^{11}C]DTBZ–[^{11}C]FMZ studies ($n = 6$) with ST studies ($n = 3$). (**C**) Comparison of dual-tracer [^{11}C]FMZ–[^{11}C]PMP studies ($n = 19$) with ST studies ($n = 10$ for [^{11}C]FMZ and $n = 9$ for [^{11}C]PMP). Error bars represent the s.d. of the estimated parameters. The regions of interest for FMZ are OCC: occipital cortex, LAT: lateral frontal cortex, SUP: superior parietal cortex, TEM: lateral temporal cortex, CAU: caudate nucleus, THA: thalamus, CER: cerebellar hemisphere, and PONS: pons. The regions of interest for DTBZ are PUT: putamen, CAU: caudate nucleus, MID: midbrain, CER: cerebral hemisphere, THA: thalamus, PONS: pons, SUP: superior parietal cortex, and OCC: occipital cortex. The regions of interest for PMP are OCC: occipital cortex, LAT: lateral frontal cortex, SUP: superior parietal cortex, TEM: lateral temporal cortex, INS: insular cortex, HIPP: hippocampus, THA: thalamus, and AMY: amygdala.

protocol as in Figure 2. The left-most column for each tracer shows the *DVR* images obtained from a ST scan. The middle and the right-most columns for each tracer show *DVR* images obtained from the dual-tracer studies using EM and SM, respectively. As ST scans were performed using only one of the two tracers used in the dual-tracer study, the images seen in the left and right halves of Figure 4 are from different subjects. The dual-tracer scans analyzed using EM and SM yielded images very close in quality to those obtained from ST scans. The image quality tended to improve when the two tracers were separated by 30 instead of 20 mins, as increasing tracer separation improves signal separation as reported for dual-tracer studies using arterial plasma inputs (Koeppe *et al*, 2001).

The bar graphs in Figure 5 (panel A) show the comparison of the means and s.d. of eight regions of interest extracted from both ST and dual-tracer parametric images. On average, EM showed a positive bias in *DVR* for [^{11}C]FMZ compared with ST, which can be primarily attributed to the fact that 20 mins of data were insufficient to accurately estimate the transport and binding parameters of the first tracer. As would be expected, the slight positive bias in the *DVR* estimates of FMZ propagates as a slight negative bias in DTBZ estimates. The magnitude of the DTBZ bias is less pronounced because for this tracer combination, the [^{11}C]DTBZ signal is the dominant contributor to the dual-tracer data (see Figure 2). The intersubject variance of the dual-tracer methods was only slightly higher on

average than that seen in the ST parametric images, indicating that image quality did not suffer because of excessive noise propagation in the dual-tracer approach. Pair-wise *t*-tests (EM versus SM, EM versus ST, and SM versus ST) showed that for the first tracer, EM was significantly higher than SM ($P<0.001$ for all cortical regions), EM was significantly higher than ST ($P<0.05$ in 3 of 4 cortical regions), and that there was no significant difference between the SM and ST for all regions ($P=0.15$ to $P=0.40$). However, for the second tracer, no significant difference was seen between the three sets.

[^{11}C]DTBZ–[^{11}C]FMZ Studies

Figure 4 (panel B) shows parametric images from studies, in which [^{11}C]DTBZ was injected first, followed by [^{11}C]FMZ. Again, the dual-tracer methods were successful in accurately separating the individual-tracer signals as indicated by the similarity of ST and either the EM and SM parametric images. Similar to the [^{11}C]FMZ–[^{11}C]DTBZ case, images for the EM have higher values than those in the ST scan, whereas the same scan analyzed with SM yielded results closer to those of the ST scan.

Figure 5 (panel B) shows trends similar to those seen in panel A, including the positive bias in EM *DVR* values for the first tracer, which in this protocol was [^{11}C]DTBZ. As before, the intersubject region-of-interest variance for dual-tracer methods was similar or only slightly higher than that seen in the ST images, again indicating that image quality in dual-tracer PET is not degraded substantially by the propagation of noise. Pair-wise *t*-tests showed that for the first tracer, EM was significantly higher than SM ($P<0.002$ for both the caudate nucleus and the putamen), and EM values were further away from ST values than those from SM. However, there was no significant difference either between EM and ST or between SM and ST ($P=0.15$ to $P=0.35$). For the second tracer, there were no significant differences between the three sets.

[^{11}C]FMZ—[^{11}C]PMP Studies

Figure 4 (panel C) shows parametric images for a study, in which [^{11}C]FMZ was injected 30 mins before [^{11}C]PMP. Estimation of the trapping constant for [^{11}C]PMP using the RLS (Nagatsuka *et al*, 2001) breaks down in the areas of high trapping because of the ill-conditioned nature of the operational equation (Equation 14). This can be seen in both the ST and dual-tracer k_3 images. AChE activity has a very large dynamic range in the human brain, and as the primary regions of interest for PMP are in the cortex, the images are scaled to better show these values rather than the cerebellum (vermis) and brainstem structures, which appear as white in the parametric images.

The bar graphs for [^{11}C]FMZ (Figure 5, panel C) showed the familiar features seen in panels A and B, such as positively biased *DVR* estimates for EM and a much less-pronounced bias for SM-based *DVR* estimates. The EM-based bias is less for the trapping constant estimation. However, the estimation of k_3 from signals extracted using SM is negatively biased in most regions compared with the ST 'gold standard' values. The intersubject region-of-interest variance for EM and SM was similar to that seen in ST images for [^{11}C]FMZ, but was higher for [^{11}C]PMP. For [^{11}C]PMP, the variance in the dual-tracer methods was larger than that in ST studies for regions, such as the thalamus and amygdala that have higher AChE activity. Pair-wise *t*-tests showed that for the first tracer, EM was significantly higher than SM ($P<0.0002$ for all cortical regions) and EM values were further away from ST than SM, SM values were not significantly different than ST ($P>0.1$), whereas EM values were significantly higher than ST ($P<0.005$). For the second tracer, unlike the earlier tracer pairs, EM was significantly higher than SM ($P<0.05$ for 3 of 4 cortical regions), whereas there were no significant differences for either EM or SM and ST.

Discussion

This paper presents the first results of human dual-tracer brain PET studies carried out noninvasively using reference tissue approaches, hence not requiring arterial blood sampling and plasma metabolite analyses. This noninvasive approach can provide information on two distinct biologic systems from a single PET scan. As the various neurotransmitter systems of the brain do not act in isolation but have complex interactions, dual-tracer methods can be particularly useful in 'challenge' studies, in which the effect of a pharmacological or behavioral intervention may be on more than a single neuropharmacological system.

The key assumption for this methodology is that the first radiotracer can be brought to steady state before injection of the second radiotracer. This assumption allows one to know the full time course of the reference tissue for the first radiotracer, which acts as the 'input function' for the reference tissue model. In general, both reversible and irreversible tracers that satisfy the above criterion could be injected first. However, in this study, the irreversible tracer, [^{11}C]PMP, could not be used first as it had no region that was void of AChE. Rapidly equilibrating tracers, such as flumazenil, used in this study, or raclopride, would be expected to work well, whereas the more slowly equilibrating tracers, such as methylphenidate or carfentanil, would be poor choices for the 'first' tracer.

Of the two evaluated analysis approaches, EM, although intuitive, seems to introduce bias in many studies, as parameter estimates derived from only 20 to 30 mins of data can be insufficient for robust

parameter estimation. Furthermore, biases in the parameter estimates for the first tracer will propagate as biases in the parameter estimates of the second tracer. The biases in the two tracers, in general, will be negatively correlated, as an error in the TAC estimation of the first tracer would be compensated by an opposite error in the TAC of the second tracer, for the sum of the individual-tracer curves to fit the dual-tracer curve. Thus, to avoid the limitations of the EM approach, a SM was developed and evaluated. In the majority of cases, an improvement of the simultaneous method over EM was seen in terms of better correspondence of the *DVR* measures with those of the ST scans. This was achieved by fitting the dual-tracer TACs with a combined reference tissue model, to optimally separate the total PET signal into its two 'single-tracer' components. A possible remaining source of bias in the SM approach is that before the simultaneous fit, the reference tissue TAC for the second tracer must be determined for which the extrapolation approach was still needed. Once the second reference tissue curve is obtained, the TACs for all voxels can be separated. One aspect of our implementation of the simultaneous method is that after separation of the dual-tracer scan into its individual-tracer image sequences, one can redefine the reference-tissue curves on the separated data sets.

One of the primary concerns in any dual-tracer approach is the need to estimate approximately twice as many parameters as compared with a ST PET study. Although at first glance, this may seem to be a prohibitive problem, the fact that administration of the two tracers is offset in time provides considerably more 'kinetic' information in a dual-tracer curve than in a ST curve. However, trying to estimate 6 to 8 parameters from an 80-min PET session is more challenging that estimating 2 to 3 parameters from a ST scan, and precision of the parameter estimates is a concern. Thus, we made efforts along three fronts to enhance precision for providing more robust results.

First, we reduced the voxel-level noise in the TACs using a simple adaptive smoothing procedure. The choice of the threshold for this step must be made carefully, as too high a threshold would result in little smoothing, hence little improvement in precision, whereas too low a threshold would result in overly degrading the effective spatial resolution of the parametric images. The success of this approach can be seen in the parametric images shown in Figures 3 and 4. In all cases, the apparent noise level is nearly as low for dual-tracer studies as for ST scans.

Second, we fixed the k_4 parameter of the full-reference tissue model for both tracers to the population average values during the fitting procedure for separating the dual-tracer signal into its individual components. Using the full-reference tissue model (four parameters, for each tracer), yet fitting only three parameters per tracer, helped to stabilize the fit while maintaining a model formulation with more realistic shapes for the tracers' TACs.

Third, while reducing the number of fitted parameters improved the ability to extract ST curves, using the direct parameter estimates to calculate *DVR* ($=1+k_3/k_4$) with good precision is still limited. This is similar to ST studies, in which more stable estimates of *DVR* can usually be obtained by methods, such as the Logan plots, rather than directly using nonlinear least squares estimates of individual rate parameters for the calculation of *DVR*. Hence, in this study, application of the robust linear Logan graphical analysis was used after the separation of individual-tracer signals to obtain estimates of the parameters of interest, *DVR* (RLS for k_3) and R_1. As the separated tissue TACs were obtained as smooth curves, the potential biases in *DVR* estimates because of noisy data were avoided.

As expected, increasing the time offset between tracer injections from 20 to 30 mins provided an improvement in the precision for both EM and SM approaches. However, this is a trade-off that would have to be considered for any dual-tracer application. Minimizing the time difference between the administrations of the two tracers would provide a more simultaneous estimation of the tracer parameters, but would decrease the precision of parameter estimates. Conversely, increasing the time difference between tracer injections, while improving precision in parameter estimates, would increase the chance that the biologic or pharmacological state of the subject would change. This may be problematic especially in 'challenge' studies, in which one assumes that a variety of biologic parameters (blood flow, endogenous neurotransmitter levels, receptor occupancy) are constant over time.

Pair-wise *t*-tests between the three methods (ST, EM, SM) showed that for the first tracer, SM in general was better than EM and closer to the ST results, whereas for the second tracer, the performance of SM and EM was not significantly different from that of ST.

In conclusion, noninvasive dual-tracer methodology has been shown to produce results comparable with ST scans, and promises to be a very useful technique for a near simultaneous evaluation of multiple brain systems from a single PET acquisition.

Conflict of interest

The authors declare no conflict of interest.

References

Black NF, McJames S, Rust TC, Kadrmas DJ (2008) Evaluation of rapid dual-tracer (62)Cu-PTSM + (62)Cu-ATSM PET in dogs with spontaneously occurring tumors. *Phys Med Biol* 53:217–32

Comtat C, Kinihan PE, Defrise M, Michel C, Townsend DW (1998) Fast reconstruction of 3D data with accurate statistical modeling. *IEEE Trans Nucl Sci* 45:1083–9

Cunningham VJ, Hume SP, Price GR, Ahier RG, Cremer JE, Jones AK (1991) Compartmental analysis of diprenorphine binding to opiate receptors in the rat in vivo and its comparison with equilibrium data in vitro. *J Cereb Blood Flow Metab* 11:1–9

Defrise M, Kinihan PE, Townsend DW, Michel C, Sibomana M, Newport DF (1997) Exact and approximate rebinning algorithms for 3-D PET data. *IEEE Trans Med Imaging* 16:145–58

Faraway J (2004) Weighted Least Squares. In: *Linear Models with R*. Chapman & Hall/CRC: Boca Raton, pp 92–4

Frey KA, Groom GN, Minoshima S, Koeppe RA, Kuhl DE (1993) True equilibrium quantification of human cerebral benzodiazepine receptors with the use of [11-C]flumazenil and positron tomography. *J Nucl Med* 34:108P

Herholz K, Lercher M, Wienhard K, Bauer B, Lenz O, Heiss WD (2001) PET measurement of cerebral acetylcholine esterase activity without blood sampling. *Eur J Nucl Med* 28:472–7

Holthoff VA, Koeppe RA, Frey KA, Paradise AH, Kuhl DE (1991) Differentiation of radioligand delivery and binding in the brain: validation of a two-compartment model for [11C]flumazenil. *J Cereb Blood Flow Metab* 11:745–52

Huang SC, Carson RE, Hoffman EJ, Kuhl DE, Phelps ME (1982) An investigation of a double-tracer technique for positron computerized tomography. *J Nucl Med* 23:816–22

Hudson HM, Larkin RS (1994) Accelerated image reconstruction using ordered subsets of projection data. *IEEE Trans Med Imaging* 13:601–9

Innis RB, Cunningham VJ, Delforge J, Fujita M, Gjedde A, Gunn RN, Holden J, Houle S, Huang SC, Ichise M, Iida H, Ito H, Kimura Y, Koeppe RA, Knudsen GM, Knuuti J, Lammertsma AA, Laruelle M, Logan J, Maguire RP, Mintun MA, Morris ED, Parsey R, Price JC, Slifstein M, Sossi V, Suhara T, Votaw JR, Wong DF, Carson RE (2007) Consensus nomenclature for in vivo imaging of reversibly binding radioligands. *J Cereb Blood Flow Metab* 27:1533–9

Joshi AD, Fessler JA, Koeppe RA (2008) Improving PET receptor binding estimates from Logan plots using principal component analysis. *J Cereb Blood Flow Metab* 28:852–65

Kadrmas DJ, Rust TC (2005) Feasibility of rapid multitracer PET tumor imaging. *IEEE Trans Nucl Imag* 52:1341–7

Koeppe RA, Frey KA, Kuhl DE, Kilbourn MR (1999*a*) Assessment of extrastriatal vesicular monoamine transporter binding site density using stereoisomers of [11C]dihydrotetrabenazine. *J Cereb Blood Flow Metab* 19:1376–84

Koeppe RA, Frey KA, Kume A, Albin R, Kilbourn MR, Kuhl DE (1997) Equilibrium versus compartmental analysis for assessment of the vesicular monoamine transporter using (+)-alpha-[11C]dihydrotetrabenazine (DTBZ) and positron emission tomography. *J Cereb Blood Flow Metab* 17:919–31

Koeppe RA, Frey KA, Snyder SE, Meyer P, Kilbourn MR, Kuhl DE (1999*b*) Kinetic modeling of N-[11C]methylpiperidin-4-yl propionate: alternatives for analysis of an irreversible positron emission tomography trace for measurement of acetylcholinesterase activity in human brain. *J Cereb Blood Flow Metab* 19:1150–63

Koeppe RA, Frey KA, Vander Borght TM, Karlamangla A, Jewett DM, Lee LC, Kilbourn MR, Kuhl DE (1996) Kinetic evaluation of [11C]dihydrotetrabenazine by dynamic PET: measurement of vesicular monoamine transporter. *J Cereb Blood Flow Metab* 16:1288–99

Koeppe RA, Holthoff VA, Frey KA, Kilbourn MR, Kuhl DE (1991) Compartmental analysis of [11C]flumazenil kinetics for the estimation of ligand transport rate and receptor distribution using positron emission tomography. *J Cereb Blood Flow Metab* 11:735–44

Koeppe RA, Joshi A, Frey K, Snyder SE, Kilbourn MR, Fessler J (2004) Dual-tracer PET studies without arterial sampling. *NeuroImage* 22:T115–6

Koeppe RA, Raffel DM, Snyder SE, Ficaro EP, Kilbourn MR, Kuhl DE (2001) Dual-[^{11}C]tracer single-acquisition positron emission tomography studies. *J Cereb Blood Flow Metab* 21:1480–92

Lammertsma AA, Bench CJ, Hume SP, Osman S, Gunn K, Brooks DJ, Frackowiak RS (1996) Comparison of methods for analysis of clinical [11C]raclopride studies. *J Cereb Blood Flow Metab* 16:42–52

Lammertsma AA, Hume SP (1996) Simplified reference tissue model for PET receptor studies. *Neuroimage* 4:153–8

Logan J, Fowler JS, Volkow ND, Ding YS, Wang GJ, Alexoff DL (2001) A strategy for removing the bias in the graphical analysis method. *J Cereb Blood Flow Metab* 21:307–20

Minoshima S, Koeppe RA, Frey KA, Kuhl DE (1994) Anatomical standardization: linear scaling and nonlinear warping of functional brain images. *J Nucl Med* 35:1528–37

Minoshima S, Koeppe RA, Mintun MA, Berger KL, Taylor SS, Frey KA, Kuhl DE (1993) Automated detection of the intercommissural (AC-PC) line for stereotactic localization of functional brain images. *J Nucl Med* 34:322–9

Nagatsuka S, Fukushi K, Shinotoh H, Namba H, Iyo M, Tanaka N, Aotsuka A, Ota T, Tanada S, Irie T (2001) Kinetic analysis of [(11)C]MP4A using a high-radioactivity brain region that represents an integrated input function for measurement of cerebral acetylcholinesterase activity without arterial blood sampling. *J Cereb Blood Flow Metab* 21:1354–66

Rust TC, DiBella EV, McGann CJ, Christian PE, Hoffman JM, Kadrmas DJ (2006) Rapid dual-injection single-scan 13N-ammonia PET for quantification of rest and stress myocardial blood flows. *Phys Med Biol* 51:5347–62

Rust TC, Kadrmas DJ (2006) Rapid dual-tracer PTSM+ATSM PET imaging of tumour blood flow and hypoxia: a simulation study. *Phys Med Biol* 51:61–75

Talairach J, Tournoux P (1988) *Co-planar Stereotaxic Atlas of the Human Brain: 3-Dimensional Proportional System - an Approach to Cerebral Imaging*. New York, NY: Thieme Medical Publishers